

## Scaling Characteristics of Azimuthal Anisotropy at RHIC

Michael Issah<sup>1</sup> and Arkadij Taranenko<sup>1</sup>, for the PHENIX Collaboration

<sup>1</sup> Department of Chemistry, State University of New York at Stony Brook, Stony Brook, New York 11794-3400, USA

**Abstract.** Recent differential measurements of elliptic flow are used to probe several hydrodynamic scaling predictions. Eccentricity scaling is observed for Cu+Cu and Au+Au collisions at  $\sqrt{s_{NN}} = 200$  GeV, suggesting essentially complete thermalization of the high energy density matter produced in these collisions. An estimate of the speed of sound is also obtained from the eccentricity scaled elliptic flow. The predicted mass scaling is observed for particles with transverse kinetic energy  $KE_T$  up to  $\sim 1$  GeV. For  $KE_T$  values above  $\sim 1$  GeV, valence quark number scaling compatible with partonic degrees of freedom is observed.

*Keywords:* RHIC, PHENIX, azimuthal anisotropy, eccentricity scaling, speed of sound, coalescence, transverse kinetic energy

*PACS:* 01.30.Cc, 12.38.Mh, 24.85.+p, 25.75.Nq, 25.75.Ld

### 1. Introduction

Experimental measurements at the Relativistic Heavy Ion Collider (RHIC) have indicated the creation of matter having energy density in excess of what is required for the formation of a de-confined phase of quarks and gluons (QGP) [ 1, 2, 3]. The decay of this matter results in particle emissions which show large anisotropies in their azimuthal distributions relative to the reaction plane. Such anisotropies, which are commonly characterized by the second Fourier coefficient  $v_2$ , suggest that the created high-energy density matter rapidly thermalizes and its decay dynamics is driven by substantial pressure gradients throughout its dynamical evolution [ 4, 5, 6].

This picture for the matter created in RHIC collisions is supported by the good agreement achieved between  $v_2$  measurements [ 7, 8, 9, 10, 11, 12] and those obtained from hydrodynamic model calculations [ 13, 14, 16]. However, the detailed properties of the matter (ie. its equation of state, transport coefficients, effective

degrees of freedom, etc), are still lacking. Recently, several questions concerning the degree of thermalization of this matter have even been under debate [ 15, 16].

In this contribution, we show that the scaling characteristics of azimuthal anisotropy provide an important framework for developing important insights relevant to the properties of the high energy density matter created in ultrarelativistic heavy ion collisions at RHIC.

## 2. Data & data analysis

The results presented here utilize data obtained by the PHENIX collaboration for the Au+Au and Cu+Cu colliding systems at  $\sqrt{s_{NN}}=200$  GeV. A detailed description of the PHENIX detector is given elsewhere [ 17]. The procedures for tracking and event selection are described in Refs. [ 9, 11]. The azimuthal anisotropies relevant to this work were measured using the reaction plane method [ 18, 19, 20]. This method measures the correlations between the azimuthal angle of the particles detected in the central arms of PHENIX and the azimuth of the reaction plane obtained with the two Beam-Beam Counters (BBC) located at  $|\eta| \sim 3 - 3.9$  [ 9]. An important advantage of the large  $\eta$  separation between the BBC's and the central arms of PHENIX is the expectation that the evaluation of the azimuth of the reaction plane is much less affected by possible non-flow contributions, especially those due to jets[ 9].

The magnitude of these elliptic flow correlations was determined by evaluating the second Fourier coefficient  $v_2$ , of the azimuthal distribution of emitted particles relative to the azimuth of the reaction plane [ 18, 19, 20]:

$$v_2 \equiv \langle e^{2i(\phi - \Phi_{RP})} \rangle = \langle \cos 2(\phi - \Phi_{RP}) \rangle. \quad (1)$$

Here,  $\phi$  is the azimuthal angle of a particle measured in the laboratory coordinate system and  $\Phi_{RP}$  is an estimate of the azimuth of the reaction plane. A resolution factor was evaluated and used to correct for the dispersion of the measured reaction plane about the true reaction plane.

Detailed measurements were performed over a broad range of centralities,  $p_T$  and particle species. The results from these measurements are presented in the following sections.

## 3. Insights into the degree of thermalization

### 3.1. Eccentricity scaling

As mentioned earlier, the large  $v_2$  values measured at RHIC [ 7, 8, 9, 10, 11, 12] are compatible with those obtained from hydrodynamic model calculations [ 13, 14, 16]. Local thermalization constitutes an important assumption for the legitimate use of hydrodynamics to describe the data. This being so, a crucial question is whether or not one can gain further insights into the degree of thermalization from the data.

To do this, we recall here that an important prediction of the hydrodynamic model is that  $v_2$  should (i) scale with eccentricity and (ii) be independent of the colliding system for a given eccentricity [ 15, 16, 21]. The eccentricity  $\epsilon = \langle y^2 \rangle - \langle x^2 \rangle / (\langle y^2 \rangle + \langle x^2 \rangle)$ , measures the asymmetry of the “almond shaped” collision zone containing the high energy density matter created in the collision;  $x$  and  $y$  are, respectively, the short and long axes of the almond.

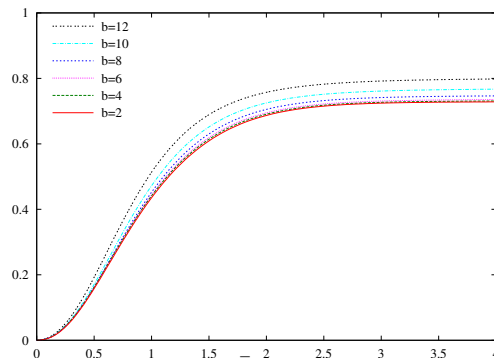


**Fig. 1.**  $v_2/\epsilon$  as a function of  $c_s(t-t_0)/\bar{R}$  for different impact parameters. The plot is taken from [ 15].

The eccentricity scaling prediction of hydrodynamics is illustrated in Fig. 1. The figure shows that, for a system of transverse size  $\bar{R}$ , elliptic flow develops over a time scale  $\sim \bar{R}/\langle c_s \rangle$  for matter with a speed of sound  $c_s$  [ 15]. More importantly, it shows the variation of the scaled anisotropy  $v_2/\epsilon$ , as a function of the characteristic distance  $c_s(t-t_0)/\bar{R}$ , where  $t_0$  is the thermalization time. The scaled results, which are shown for several impact parameters  $b$  or centralities, are taken from Ref. [ 15]. They indicate that  $v_2/\epsilon$  is essentially independent of centrality except for the most peripheral collisions, where hydrodynamics is expected to break down. This result provides a clear signature for hydrodynamic scaling which can be explored with data.

The left panels of Fig. 2 show recently measured differential elliptic flow  $v_2(p_T)$  for several centralities in Au+Au and Cu+Cu collisions at  $\sqrt{s_{NN}}=200$  GeV. For both systems, the characteristic increase of  $v_2(p_T)$  as collisions become more peripheral is evident. In a hydrodynamic scenario, this increase is expected because  $\epsilon$  grows as collisions become less central and larger values of  $\epsilon$  lead to larger pressure gradients which drive the magnitude of collective flow. The crucial question here is whether or not these data show the eccentricity scaling predicted by hydrodynamic models.

The right panel of Fig. 2 shows the scaled values of  $v_2(p_T)$  for the same centralities shown in the left panel of the figure. To estimate the eccentricity, we use the fact that the  $p_T$ -integrated  $v_2$  values vary linearly with centrality and are essentially proportional to  $\epsilon$ , i.e  $\epsilon \sim k \times v_2$  over a broad range of centrality selections. Here,

it should be emphasized that this proportionality has been experimentally verified in Au+Au collisions [ 7, 8]. From Glauber model estimates [ 7] of  $\epsilon$ , we find that  $k \sim 3$  for the cuts employed in this analysis. This factor is reflected in the right panel of Fig. 2 where we have used  $v_2(p_T)/3v_2(\text{centrality})$  for the scaled anisotropy. This ratio has the added advantage of being less affected by the systematic errors associated with our  $v_2$  measurements since they cancel out.

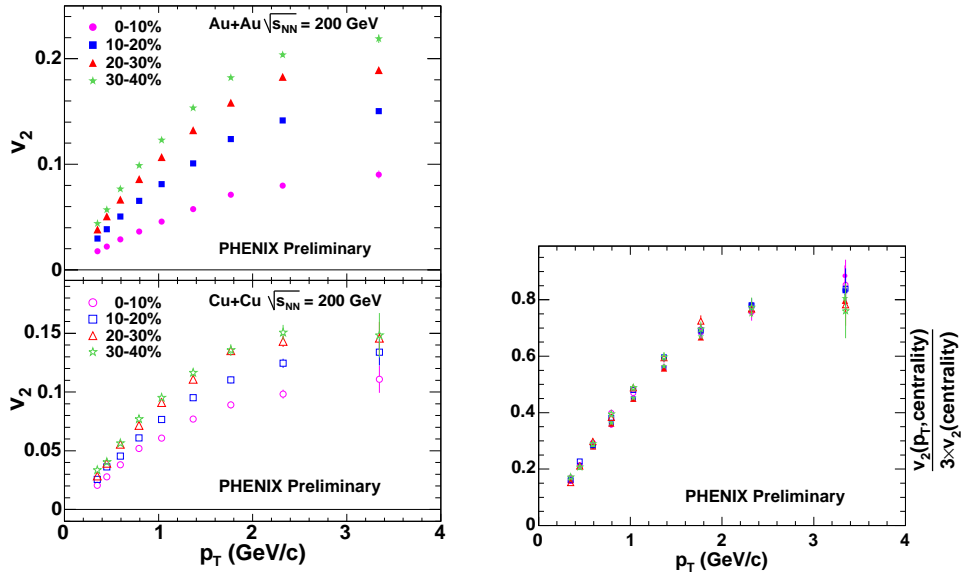


**Fig. 2.** The left panels show  $v_2$  vs.  $p_T$  for several centrality selections for Au+Au (top) and Cu+Cu (bottom) collisions at  $\sqrt{s_{NN}} = 200$  GeV. The right panel shows  $v_2(p_T)$  scaled by the  $p_T$ -integrated  $v_2$  values for the same centralities indicated in the left panels.

The scaled  $v_2$  values shown in the right panel of Fig. 2 indicate rather good scaling for the full range of centralities (or  $\epsilon$ ) presented. This is clearly consistent with the eccentricity scaling predictions of hydrodynamics. Equally important is the fact that these results also confirm the expected independence on colliding system size.

We interpret these findings as an indication that essentially full thermalization is achieved over a broad set of these Au+Au and Cu+Cu collisions [ 12, 15]. The observation of the independence of  $v_2/\epsilon$  on the system size also satisfies the requirement of scale invariance which is a basic feature of perfect fluid hydrodynamics.

Given these observations, it is important to ask whether or not one can use them to extract constraints for the properties of the high energy density matter. This is pursued in the next section.

### 3.2. An estimate of the speed of sound from scaled $v_2$ data

An important input for the hydrodynamic model is the equation of state (EOS). The EOS relates the pressure  $p$  to the energy density  $\varepsilon$ . For a simple EOS,  $p = c_s^2 \varepsilon$ . Since  $v_2$  is driven by pressure gradients in the hydrodynamical model, the value of the speed of sound  $c_s$  can greatly influence the magnitude of  $v_2$ .

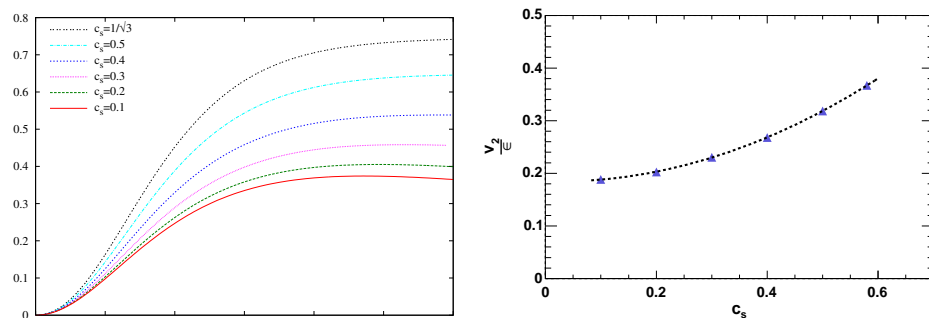


**Fig. 3.** The left panel shows  $v_2/\varepsilon$  as a function of  $c_s(t-t_0)/\bar{R}$  for various values of  $c_s$ . The calculation was performed for Au+Au collisions with impact parameter  $b = 8$  fm at  $\sqrt{s_{NN}} = 200$  GeV [ 15]. The right panel gives a summary of the dependence of  $v_2/\varepsilon$  on  $c_s$ . The dotted curve is represent a fit to the simulated data.

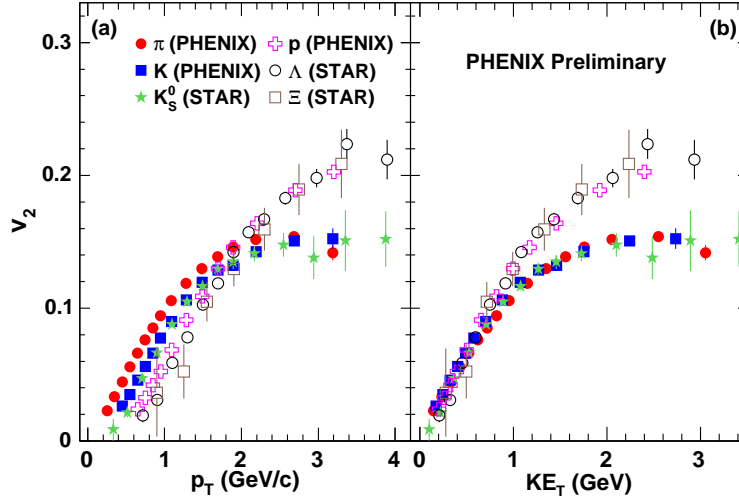
The results from a recent study of the influence of  $c_s$  on the magnitude of  $v_2/\varepsilon$  [ 15, 21] is shown in Fig. 3. The figure indicates that the magnitude of  $v_2/\varepsilon$  is rather sensitive to the assumed value for  $c_s$ . This sensitivity is made more transparent in the right panel of Fig. 3 where we have summarized the results.

An estimate of the speed of sound can be made by comparing the eccentricity scaled  $v_2$  values shown in Fig. 2, with the model predictions shown in Fig. 3. It is noteworthy that we have checked that the eccentricities used in the model are comparable to Glauber based model estimates [ 7] used in our evaluation of  $k$ . It should be pointed out that the  $v_2/\varepsilon$  values in the left panel of Fig. 3 differ from those in the right panel by a factor of 2. This factor was applied to take account of a well known difference in the procedure used to evaluate  $v_2$  from the data and theory [ 15]. A comparison between the right panels of Figs. 2 and 3 gives the estimate  $c_s \sim 0.35 \pm 0.05$  for a  $\langle p_T \rangle \sim 0.45$  GeV/c [ 22]. This value of  $c_s$  is indicative of a soft equation of state [ 11]), with the matter possibly spending little time, during its evolution, in a region where  $c_s = 0$ .

### 3.3. Transverse kinetic energy scaling

Given the observed eccentricity scaling, one can try to explore other hydrodynamic scaling scenarios. For instance, the variation of  $v_2$  with transverse kinetic energy  $\text{KE}_T = m_T - m$ , where  $m_T = \sqrt{p_T^2 + m^2}$  is the transverse mass of the particle, is a

good candidate for study. The use of this variable is intuitive because pressure gradients, which give rise to azimuthal anisotropy, lead to collective transverse kinetic energy of the emitted particles.



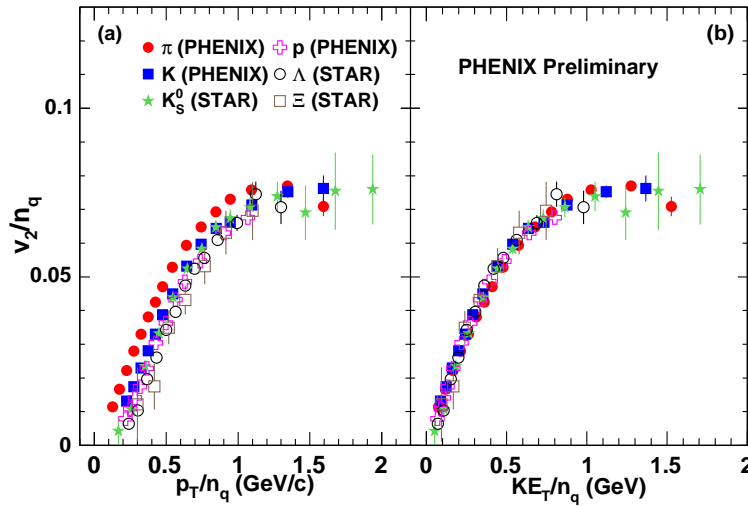
**Fig. 4.** Variation of  $v_2$  with (a)  $p_T$  and (b)  $KE_T$  for selected hadrons for minimum bias collisions. The pion ( $\pi^\pm$ ), kaon ( $K^\pm$ ) and (anti-)proton ( $(\bar{p})p$ ) results are from PHENIX [ 23] and the neutral kaon  $K_0^S$ , lambda  $\Lambda$  and cascade  $\Xi$  results are from STAR [ 24].

Figure 4 shows the dependence of  $v_2$  on  $p_T$  and  $KE_T$  (respectively) for several identified particles. The values of  $v_2$  for charged pions ( $\pi^\pm$ ), kaons ( $K^\pm$ ) and (anti-)protons ( $(\bar{p})p$ ) are preliminary data from the PHENIX Collaboration [ 12, 23] whereas those for  $K_0^S$ ,  $\Lambda$  and  $\Xi$  are published data from STAR Collaboration [ 24]. The STAR  $v_2$  values were multiplied by a factor of 1.1 to account for a small difference in the mean centrality for minimum bias events measured by the two experiments. In the left panel of Fig. 4, one can observe mass ordering of  $v_2(p_T)$  for  $p_T$  up to  $\sim 2$  GeV/c. That is, for a given  $p_T$ , the larger the mass of a particle, the smaller its  $v_2$ . This pattern has been identified as a signature for hydrodynamic expansion [ 25].

In the right panel of Fig. 4,  $v_2$  is plotted as a function of  $KE_T$ . Here, it can be seen that  $v_2(KE_T)$  shows the expected scaling with  $KE_T$  up to  $\sim 1$  GeV. For larger values of  $KE_T$ , the scaling breaks. However, a rather striking trend emerges : the mesons and baryons scale independently for the whole  $KE_T$  range. This pattern suggests that the constituents of which baryons and mesons are made also flow. We pursue this lead via an additional scaling test in the next section.

#### 4. What are the degrees of freedom in the high energy density matter ?

The observation in Fig. 4 that mesons and baryons scale in two separate branches for  $KE_T$  values above  $\sim 1$  GeV suggests that the constituents of the hadrons flow. If this is indeed the case, then the data should reflect constituent quark number scaling. Indeed, several models based on the coalescence or recombination of constituent quarks have been developed [ 26, 27, 28, 29, 30]. In these models, mesons and baryons obtain their elliptic flow from the elliptic flow of partons in an additive way, so that we have the simple relations:  $v_{2,M}(p_T) \simeq 2 v_{2,p}(p_T/2)$  and  $v_{2,B}(p_T) \simeq 3 v_{2,p}(p_T/3)$ , where  $v_{2,M}$ ,  $v_{2,B}$  and  $v_{2,p}$  are the  $v_2$  of a meson, baryon and parton respectively. The underlying assumption of this picture is that each parton carries the same fraction of the hadron elliptic flow.



**Fig. 5.** Variation of  $v_2/n_q$  with  $p_T/n_q$  (left panel) and with  $KE_T/n_q$  (right panel) for different hadron species for minimum bias collisions.

The results from constituent quark number scaling are shown in Fig. 5. Here the values for  $v_2$ ,  $p_T$  and  $KE_T$  for different particle species are divided by their respective number of quarks for mesons ( $n_q=2$ ) and baryons ( $n_q=3$ ). The left panel shows the commonly exploited quark number scaling ansatz:  $v_2(p_T)/n_q$  vs  $p_T/n_q$ . The left panel shows poor scaling for  $p_T/n_q \leq 1$  GeV/c and better scaling, within errors, for  $p_T/n_q \geq 1.3$  GeV/c. In contrast, the right panel shows that  $v_2(KE_T)/n_q$  scales over the whole range of  $KE_T/n_q$ . This observation can be interpreted as a strong indication that the pertinent degrees of freedom in the flowing high energy density matter are linked to the number of constituent quarks of the hadron.

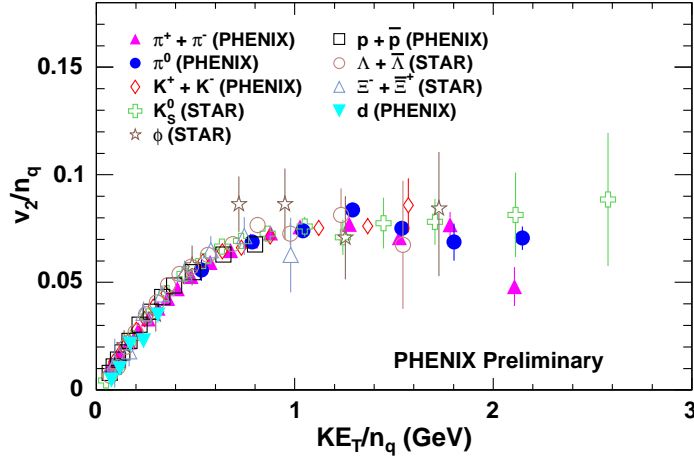


**Fig. 6.** Variation of  $v_2/n_q$  with  $KE_T/n_q$  for a comprehensive set of hadrons.

Fig. 6 shows the scaling with  $KE_T/n_q$  for a more comprehensive set of hadron species. The  $\phi$  meson and deuteron  $v_2$  values are taken from [ 31] and [ 12] respectively. It appears that the scaling holds even for a heavy meson like the  $\phi$  and for the deuteron ( $n_q=6$ ), lending support to the idea that the different particle species emerge from a common flow field.

#### 4.1. Quark number scaling for different centrality selections

Hydrodynamics is expected to break down for the most peripheral collisions and for relatively high  $p_T$  [ 13]. Consequently, it is important to investigate the evolution of the scaling picture as the centrality of collisions is varied and the  $p_T$  of the particles is increased. Such an analysis is still under intense investigation. Nonetheless, we show preliminary scaling results for a select set of centralities in Fig. 7. Interestingly, quark number scaling of  $v_2$  and  $KE_T$  holds rather well for the range of centralities presented. It will be interesting to see if this scaling breaks for more peripheral collisions and at high  $p_T$ .

## 5. Conclusions

In summary, we have presented results for the scaling properties of azimuthal anisotropy at RHIC. The eccentricity scaled  $v_2$  values for Cu+Cu and Au+Au at  $\sqrt{s_{NN}} = 200$  GeV are similar as a function of  $p_T$ , showing that scale invariance of azimuthal anisotropy is satisfied. This suggests essentially complete thermalization



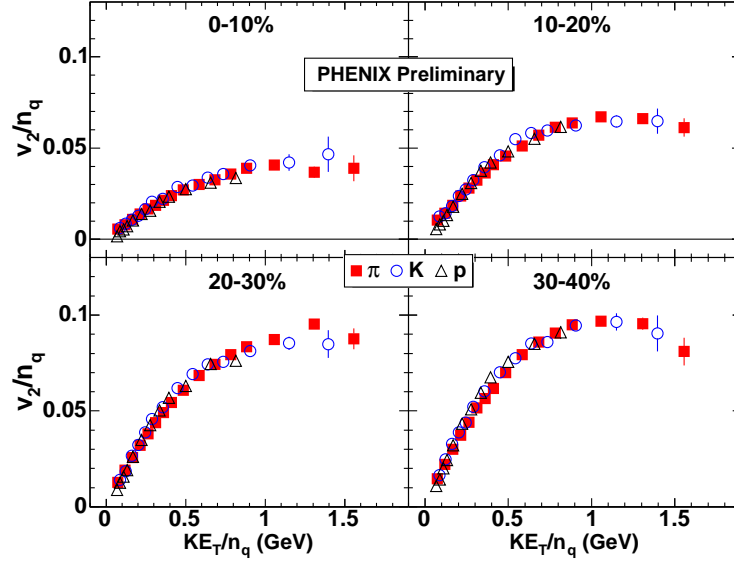


**Fig. 7.** Variation of  $v_2/n_q$  with  $KE_T/n_q$  for  $\pi^\pm$ ,  $K^\pm$  and  $p(\bar{p})$  for selected centralities for Au+Au collisions at  $\sqrt{s_{NN}} = 200$  GeV.

of the high energy density matter produced in these collisions. The variation of  $v_2$  with transverse relativistic kinetic energy  $KE_T$  shows the predicted hydrodynamic mass scaling at low  $KE_T$ . However, it evolves into a differentiation of the mesonic and baryonic flow character of particles produced with high  $KE_T$ . This suggests that  $KE_T$  is a good variable to study the dynamics of the produced matter. Further scaling of  $v_2$  and  $KE_T$  by the number of valence quarks leads to a unified scaling behavior over the whole range of  $KE_T/n_q$  spanned by the data. The observations from eccentricity and transverse kinetic energy scaling point to the production of thermalized high energy density matter with partonic degrees of freedom.

## 6. Acknowledgements

We thank Hiroshi Masui and Roy Lacey for their invaluable contributions and helpful discussions.

## References

1. S. S. Adler *et al.* [PHENIX Collaboration], Phys. Rev. C **71**, 034908 (2005)

2. K. Adcox *et al.* [PHENIX Collaboration], Nucl. Phys. A **757**, 184 (2005)
3. Z. Fodor and S. D. Katz, JHEP **0203**, 014 (2002)
4. E. V. Shuryak, Nucl. Phys. A **750**, 64 (2005)
5. M. Gyulassy and L. McLerran, Nucl. Phys. A **750**, 30 (2005)
6. U. W. Heinz, arXiv:nucl-th/0504011.
7. K. Adcox *et al.* [PHENIX Collaboration], Phys. Rev. Lett. **89**, 212301 (2002)
8. C. Adler *et al.* [STAR Collaboration], Phys. Rev. C **66**, 034904 (2002)
9. S. S. Adler *et al.* [PHENIX Collaboration], Phys. Rev. Lett. **91** (2003) 182301
10. J. Adams *et al.* [STAR Collaboration], Phys. Rev. C **72** (2005) 014904
11. S. S. Adler *et al.* [PHENIX Collaboration], Phys. Rev. Lett. **94**, 232302 (2005)
12. R. A. Lacey, arXiv:nucl-ex/0510029.
13. P. F. Kolb, P. Huovinen, U. W. Heinz and H. Heiselberg, Phys. Lett. B **500** (2001) 232
14. P. Huovinen, arXiv:nucl-th/0305064.
15. R. S. Bhalerao, J. P. Blaizot, N. Borghini and J. Y. Ollitrault, Phys. Lett. B **627**, 49 (2005)
16. M. Csanad *et al.*, arXiv:nucl-th/0512078.
17. K. Adcox *et al.*, Nucl. Instrum. Meth. **A499** (2003) 469.
18. P. Danielewicz and G. Odyniec, Phys. Lett. B **157**, 146 (1985).
19. A. M. Poskanzer and S. A. Voloshin, Phys. Rev. C **58**, 1671 (1998)
20. J. Y. Ollitrault, Phys. Rev. D **48**, 1132 (1993)
21. J. Y. Ollitrault, Phys. Rev. D **46**, 229 (1992).
22. S. S. Adler *et al.* [PHENIX Collaboration], Phys. Rev. C **69**, 034909 (2004)
23. H. Masui [PHENIX Collaboration], arXiv:nucl-ex/0510018.
24. J. Adams *et al.* [STAR Collaboration], Phys. Rev. Lett. **95**, 122301 (2005)
25. P. Huovinen, P. F. Kolb, U. W. Heinz, P. V. Ruuskanen and S. A. Voloshin, Phys. Lett. B **503**, 58 (2001)
26. S. A. Voloshin, Nucl. Phys. A **715**, 379 (2003);
27. R. J. Fries, B. Müller, C. Nonaka and S. A. Bass, Phys. Rev. Lett. **90**, 202303 (2003); J. Phys. G **30**, 223 (2004).
28. V. Greco, C. M. Ko and P. Levai, Phys. Rev. Lett. **90**, 202302 (2003); Phys. Rev. C **68**, 034904 (2003).
29. D. Molnar and S. A. Voloshin, Phys. Rev. Lett. **91**, 092301 (2003).
30. R. C. Hwa and C. B. Yang, Phys. Rev. C **67**, 034902 (2003); Phys. Rev. C **67**, 064902 (2003).
31. M. Oldenburg [STAR Collaboration], arXiv:nucl-ex/0510026.

